

**Covalently Linked Acceptor–Donor Systems Based on Isoquinoline *N*-oxide Acceptor: Photoinduced Electron Transfer Produces Dual-Channel Luminescent Systems that Evolve Chemically to Photohydroxylation of the Aromatic Donor**

Daniel Collado, Ezequiel Perez-Inestrosa,\* and Rafael Suau

*Department of Organic Chemistry, Faculty of Sciences, University of Malaga, 29071-Malaga, Spain*

*inestrosa@uma.es*

*Received January 22, 2003*

Acceptor–donor compounds containing the isoquinoline *N*-oxide acceptor and (methoxy)<sub>*n*</sub>benzene (*n* = 0, 1, 2, 3) electron donors were studied. The two chromophores are connected by a CH<sub>2</sub> bridging unit. All acceptor–donor compounds exhibit photoinduced electron transfer in acid medium that results in the formation of a charge-transfer (CT) state. Measurements of the corresponding electronic emission spectra revealed that these bichromophoric systems exhibit a dual fluorescence that is strongly dependent on the protonation of the *N*-oxide function and the donor ability. The CT state responsible for the red-shifted luminescence in the studied compounds is directly connected with the initial excited state S<sub>1</sub>. On the basis of the spectroscopic and photochemical evidence, N–O bond scission is the dominant primary photochemical process involving the CT state, the subsequent radical coupling resulting in efficient aromatic hydroxylation. The outcome of both quenching and sensitization experiments confirms this assertion. The results strongly suggest that the ensuing photohydroxylation reaction is not a concerted process, but rather a two-step N–O bond scission followed by C–O bond formation, which is regioselectively guided by the electronic distribution of the resulting donor cation–radical.

**Introduction**

Electron transfer (ET) is the most elementary and ubiquitous of all chemical reactions, and plays a crucial role in many essential biological processes.<sup>1</sup> One specially significant type of ET is the photoinduced charge shift between two chromophores (or redox sites) of which one is positively charged initially (Scheme 1). These processes are classified as charge-shift electron-transfer reactions as there is no difference in net charge between the initial and final states.

The significance of these processes lies in the photoinduced generation of charge-transfer states (CT), which transforms light energy into useful chemical potentials.<sup>2</sup> The mechanistic insights derived and molecular photo-devices developed have fostered the study of systems in which the acceptor and donor groups are mutually connected via covalent linkages.<sup>3</sup> Covalently linked acceptor–spacer–donor (A–S–D) multichromophoric systems have so far been discussed largely in mechanistic terms, with emphasis on the roles of electronic and

**SCHEME 1. Photoinduced Charge Shift**



nuclear functions in determining the factors of intercomponent ET processes.<sup>4</sup>

The authors have examined a group of bichromophoric systems in which the acceptor (A<sup>+</sup>) is an isoquinoline *N*-oxide derivative, the donor (D) a benzyl derivative, and the bridge (S) a methylene group as a model system for an A<sup>+</sup>–S–D family of molecules such as **1a–g**. The photophysical behavior of these systems is of special interest since coordination of the *N*-oxide to an electrophile gives rise to a CT state emission. We recently reported the synthesis of a new type of A<sup>+</sup>–S–D podand system<sup>5</sup> and found it to be an efficient dual-channel fluorosensor for Li<sup>+</sup>, Mg<sup>2+</sup>, and Ca<sup>2+</sup>, the selectivity of the *N*-oxide coordination being crucial. Current work in this context is focusing on the research for chemical materials that can be used to develop supramolecular photochemical systems with unique properties as optical sensors and/or switches.<sup>6</sup>

The heteroaromatic *N*-oxide function is one of the few with which a monomolecular photochemical reactivity is

(1) Balzani, V., Ed. *Electron Transfer in Chemistry*; Wiley-VCH: Weinheim, Germany, 2001.

(2) Balzani, V.; Scandola, F., Eds. *Supramolecular Photochemistry*; Ellis Horwood, Ltd.: Chichester, UK, 1991.

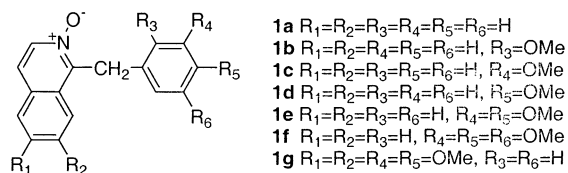
(3) (a) Closs, G. L.; Miller, J. R. *Science* **1988**, *240*, 440. (b) Jordan, K. D.; Paddon-Row, M. N. *Chem. Rev.* **1992**, *92*, 395–410. (c) Wasielewski, M. R. *Chem. Rev.* **1992**, *92*, 435–461. (d) Gust, D.; Moore, T. A.; Moore, A. L. *Acc. Chem. Res.* **1993**, *26*, 198–205. (e) Paddon-Row, M. N. *Acc. Chem. Res.* **1994**, *27*, 18–25.

(4) Reference 1, Vol. 3 and references therein.

(5) Collado, D.; Perez-Inestrosa, E.; Suau, R.; Desvergne, J.-P.; Bouas-Laurent, H. *Org. Lett.* **2002**, *4*, 855–858.

(6) Ramamurthy, V.; Schanze, K. S., Eds. *Molecular and Supramolecular Photochemistry. Vol. 7. Optical Sensors and Switches*; Marcel Dekker, Inc.: New York, 2001.

CHART 1



associated.<sup>7</sup> Reported photochemical reactions fall into two groups, i.e., rearrangement and *N*-deoxygenation.<sup>8</sup> There is now general agreement that the former involves the first excited singlet state and the latter probably the triplet state.<sup>7,9</sup> Oxygen transfer to various substrates may be an efficient intermolecular process for diazines<sup>10</sup> and polyazapolycyclic *N*-oxides.<sup>11</sup> Intramolecular oxygen transfer from pyridine *N*-oxides to bridged aromatic nuclei also has been reported.<sup>12</sup> More recently, we reported for the first time this type of photoreactivity in the bridged isoquinoline *N*-oxide derivative Papaverine *N*-oxide and showed the formation of an emissive CT state after the protonation of the *N*-oxide moiety, with ensuing intramolecular hydroxylation in high isolated yields.<sup>13</sup>

Various mechanisms have been proposed for the process, including the formation of a labile oxaziridine intermediate behaving as a strong oxidizer,<sup>14</sup> the liberation of oxygen in an active form (“oxene”),<sup>15</sup> a radical pathway,<sup>16</sup> and an electron-transfer pathway.<sup>11,13</sup> The results support the respective proposed mechanism, but some data can always inevitably be justified in terms of alternative mechanisms. Consequently, a number of questions about the reaction remain open. The importance of this reaction lies in the fact that the photolysis of aromatic *N*-oxides is used as a model for biological oxidation with monooxygenases.<sup>17</sup> Specifically, the hydroxylation of aromatics is assumed to take place via an arene oxide intermediate, as shown by using deuterated substrates, and the NIH shift mechanism is observed<sup>14a,15a</sup> as in microsomal oxidations.<sup>18</sup>

(7) Albini, A.; Pietra, S., Eds. *Heterocyclic N-oxides*; CRC Press: Boca Raton, FL, 1991.

(8) (a) Spence, G. G.; Taylor, E. C.; Buchart, O. *Chem. Rev.* **1970**, *70*, 231–265. (b) Albini, A.; Alpegiani, M. *Chem. Rev.* **1984**, *84*, 43–71. (c) Bellamy, F.; Streith, J. *Heterocycles* **1976**, *4*, 1391–1447.

(9) Tokumura, K.; Matsushita, Y. *J. Photochem. Photobiol. A: Chem.* **2001**, *140*, 27–32.

(10) Tshuchiya, T.; Ari, H.; Igeta, H. *Tetrahedron Lett.* **1970**, 2213–2216.

(11) (a) Sako, M.; Shimada, K.; Hirata, K.; Maki, Y. *Tetrahedron Lett.* **1985**, 6493–6496. (b) Sako, M.; Shimada, K.; Hirata, K.; Maki, Y. *J. Am. Chem. Soc.* **1986**, *108*, 6039–6041. (c) Sako, M.; Shimada, K.; Hirata, K.; Maki, Y. *Tetrahedron Lett.* **1986**, 3877–3880.

(12) Sammes, P. G.; Serra-Errante, G.; Tinker, A. C. *J. Chem. Soc., Perkin Trans. 1* **1978**, 853–863.

(13) Souto-Bachiller, F. A.; Perez-Inestrosa, E.; Suau, R.; Rico-Gomez, R.; Rodriguez-Rodriguez, L. A.; Coronado-Perez, M. E. *Photochem. Photobiol.* **1999**, *70*, 875–881.

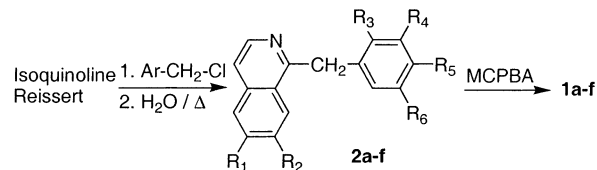
(14) (a) Akhtar, N. M.; Boyd, D. R.; Neill, J. D.; Jerina, D. M. *J. Chem. Soc., Perkin Trans. 1* **1980**, 1693–1699. (b) Kaneko, C.; Yamamori, M.; Yamamoto, A.; Hayashi, R. *Tetrahedron Lett.* **1978**, 2799–2802.

(15) (a) Ogawa, Y.; Iwasaki, S.; Okuda, S. *Tetrahedron Lett.* **1981**, 2277–2280. (b) Bucher, G.; Scaiano, J. C. *J. Phys. Chem.* **1994**, *98*, 12471–12473.

(16) Lin, S. K.; Wang, H. Q. *Heterocycles* **1986**, *24*, 659–664.

(17) (a) Streith, J.; Danner, B.; Sigwalt, C. *Chem. Commun.* **1967**, 979–980. (b) Igeta, H.; Tsuchiya, T.; Yamada, M.; Arai, H. *Chem. Pharm. Bull.* **1968**, *16*, 767–769. (c) Jerina, D. M.; Boyd, D. R.; Daly, J. W. *Tetrahedron Lett.* **1970**, 457–460.

(18) Daly, J. W.; Jerina, D. M.; Witkop, B. *Experientia* **1972**, *28*, 1129–1149.

SCHEME 2. Synthetic Methodology for the *N*-Oxides **1a–f**

In this work, we examined the photophysics and photochemistry of the benzyl derivatives of the isoquinoline *N*-oxides **1a–f** in terms of their luminescent nature and of the photoreaction products obtained. Emissive intermediate CT states were characterized and revealed that the dual-channel emissions can be modulated simply by modulating the redox properties of the acceptor and donor chromophores. The efficiency of photoinduced aromatic hydroxylation was determined and found to be unequivocally consistent with a nonconcerted hydroxyl radical mechanism.

## Results

The 1-benzylisoquinoline *N*-oxide derivatives **1a–f** were synthesized as shown in Scheme 2. By following the reported procedure,<sup>19</sup> the 1-benzylisoquinolines **2a–f** were obtained in a 70% global yield by condensation of the isoquinoline Reissert with an appropriate benzyl chloride, followed by hydrolysis. Oxidation of **2a–f** to the corresponding *N*-oxides **1a–f** was accomplished with MCPBA<sup>7</sup> in 80–90% yields.

**Steady-State Absorption Spectroscopy.** The electronic absorption spectra for compounds **1a–f** were recorded from CH<sub>2</sub>Cl<sub>2</sub> solutions and found to be very similar. The corresponding wavelength maxima and molar absorption coefficients are listed in Table 1. Figure 1 shows the electronic spectra for **1a** as a typical example; this compound exhibited a longest wavelength absorption maximum at 366 nm. In this work, we were primarily interested in this longest wavelength absorption since this weak band, which extends to 380 nm, is the *N*-oxide group  $\pi, \pi^*$  transition, of <sup>1</sup>L<sub>b</sub> symmetry and with a strong internal CT character<sup>20</sup> (a transition from a  $\pi$  orbital that is highly localized on the oxygen atom to one delocalized on the ring).<sup>21</sup>

The absorption spectra for the *N*-oxides **1a–g** are quite consistent with the combined spectra for the two-bridged units. Thus, the spectra for **1d** consist of the overlapping absorptions of isoquinoline *N*-oxide and *p*-methylanisole, except for a small 2-nm red shift in the former (Figure 2), which suggests that the covalent linkage leads to a slight electronic interaction in the ground state (weak electronic coupling). Thus, direct excitation of compounds **1a–g** with  $\lambda > 300$  nm causes an initial local excitation of the isoquinoline *N*-oxide chromophore.

**Effects of Protonation.** It has been reported that the  $\pi, \pi^*$  transition band at 366 nm for the *N*-oxide group

(19) Shamma, M. *The Isoquinoline Alkaloids. Chemistry and Pharmacology*; Academic Press: New York, 1972.

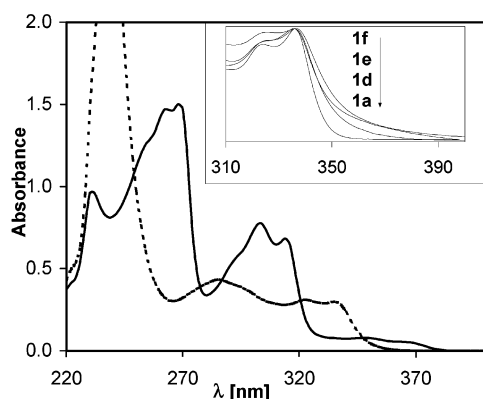
(20) Maier, J. P.; Muller, J. F.; Kubota, T.; Yamakawa, M. *Helv. Chim. Acta* **1975**, *58*, 1641–1648.

(21) (a) Brand, J. C. D.; Tang, K. T. *J. Mol. Spectrosc.* **1971**, *39*, 171–174. (b) Bist, H. D.; Parihar, J. S.; Brand, J. C. D. *J. Mol. Spectrosc.* **1976**, *59*, 435.

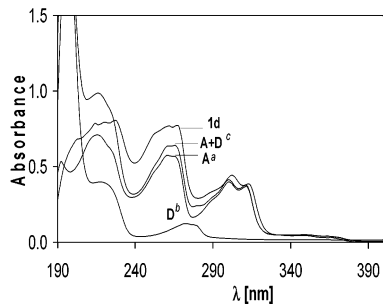
**TABLE 1.** Absorption and Fluorescence Maxima and Quantum Yields for 1a–f

		<b>1a</b>	<b>1b</b>	<b>1c</b>	<b>1d</b>	<b>1e</b>	<b>1f</b>
$\lambda_{\text{abs}}^a$ ( $\epsilon$ ) <sup>b</sup>	neutral	368 (8.9)	366 (8.4)	366 (8.7)	368 (9.5)	366 (9.5)	368 (7.9)
	acidic	336 (41.9)	336 (51.8)	336 (45.6)	336 (46.5)	336 (44.7)	336 (37.0)
$\lambda_{\text{fl}}^c$ ( $\phi$ ) <sup>d</sup>	neutral						
	$\lambda_{\text{exc}}$ 330 nm	396 (10)	394 (5)	396 (4)	394 (8)	393 (5)	399 (4)
							504 (5)
	acidic						
	$\lambda_{\text{exc}}$ 330 nm	384 (20)	380 (1)	380 (1)	380 (2)	382 (4)	380 (2)
						512 (3)	
	$\lambda_{\text{exc}}$ 366 nm	449 (18)	452 (30)	451 (20)	479 (20)	500 (54)	512 (72)

<sup>a</sup> Absorption maximum, nm. <sup>b</sup>  $\epsilon \in \% 10^{-2}$ ,  $\text{M}^{-1} \text{cm}^{-1}$ . <sup>c</sup> Emission maximum, nm. <sup>d</sup>  $\phi \times 10^3$ .

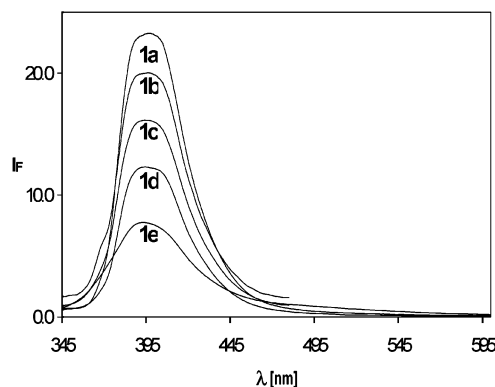


**FIGURE 1.** Electronic absorption spectra for **1a** in  $\text{CH}_2\text{Cl}_2$  (solid line) and  $\text{CH}_2\text{Cl}_2 + \text{TFA}$  (dotted line). The inset shows the 310–400-nm region for the **1a**, **1d**, **1e**, and **1f** *N*-oxides in  $\text{CH}_2\text{Cl}_2 + \text{TFA}$  solutions, normalized at 336 nm.



**FIGURE 2.** Absorption spectra for **1d**, compared with their chromophoric subunits. Absorption spectrum for a  $10^{-5}$  M  $\text{CH}_2\text{Cl}_2$  solution of **1d**. (a, b) Absorption spectra for isoquinoline *N*-oxide (acceptor subunit, A) and *p*-methylanisole (donor subunit, D) recorded from  $10^{-5}$  M  $\text{CH}_2\text{Cl}_2$  solutions. (c) Absorption spectrum for an equimolar mixture of isoquinoline *N*-oxide and *p*-methylanisole.

undergoes a strong blue shift in polar solvents,<sup>7</sup> and the spectrum in acids (0.1 M TFA in  $\text{CH}_2\text{Cl}_2$ ) is blue shifted to 336 nm (Figure 1). In addition, a weak absorption tail appears in the 340–390-nm region on the long-wavelength side of the protonated acceptor absorption. A comparison of the electronic absorption spectra for the four *N*-oxides **1a**, **1d**, **1e**, and **1f** (inset, Figure 1) reveals that electronic interaction between the chromophores increases with increasing donor ability and leads to the appearance of a new absorption band in the near-UV region. The intensity of this band is independent of the concentration. Also, lowering the donor ionization potential (from **1a** to **1f**) results in a perceived bathochromic



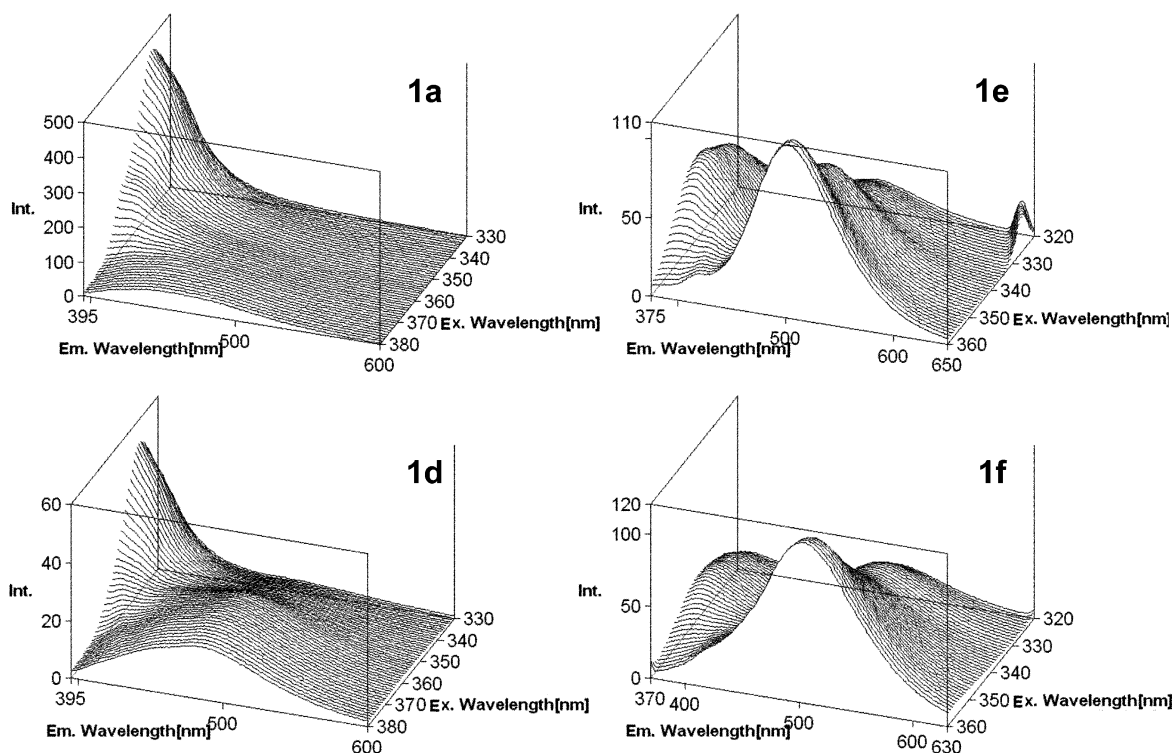
**FIGURE 3.** Fluorescence spectra for compounds **1a–e**. Curves have been scaled for clarity.

shift in this long-wavelength tail band, which is assigned to an intramolecular CT transition. However, there was substantial overlap between the relatively weak CT absorption and the strong end-absorption of the protonated acceptor moiety.

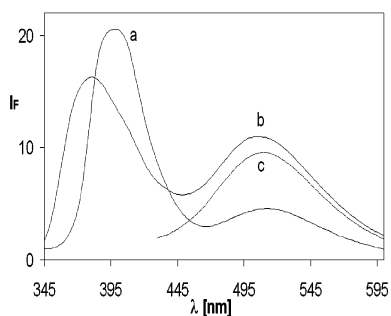
**Steady-State Fluorescence Spectroscopy.** In contrast to the absorption spectra the fluorescence spectra for the **1a–g** series exhibit differential features. Thus, the fluorescence spectra measured in  $\text{CH}_2\text{Cl}_2$  for the five first compounds **1a–e** containing the isoquinoline *N*-oxide chromophore as acceptor, and the benzene ring as the donor with zero (**1a**), one (**1b–d**), and two (**1e**) methoxy groups as substituents, exhibit a nonstructured emission band at 394 nm (Figure 3). This is the locally excited (LE) emission of the common isoquinoline *N*-oxide chromophore. It should be noted that regardless of the excitation wavelength, the same superimposable LE emission bands are observed for all compounds. This indicates that excitation at short wavelength results in energy transfer between the excited state of the donor chromophore and the ground state of the isoquinoline *N*-oxide chromophore.

In the presence of 0.1 M TFA, the emission behavior is dependent on the excitation wavelength (Figure 4). The LE emission of the protonated isoquinoline *N*-oxide is blue-shifted to 382 nm at  $\lambda_{\text{exc}} = 330$  nm and is completely displaced by a new charge transfer (CT) band beyond 400 nm at  $\lambda_{\text{exc}} > 360$  nm (Table 1).

The fluorescence spectrum for **1f** in  $\text{CH}_2\text{Cl}_2$  (Figure 5) exhibits both the LE (397 nm) and the CT (504 nm) emission profile. This latter emission is clearly enhanced by the presence of TFA. A double fluorescence emission with a decreased LE emission yield (blue shifted to 380 nm) in the protonated isoquinoline *N*-oxide chromophore



**FIGURE 4.** 3D fluorescence spectra for compounds **1a,d–f** in 0.1 M TFA  $\text{CH}_2\text{Cl}_2$  solutions.

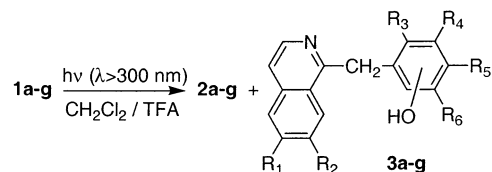


**FIGURE 5.** Fluorescence emission spectra for **1f**: (a)  $\text{CH}_2\text{Cl}_2$  solution, any  $\lambda_{\text{exc}}$ . (b)  $\text{CH}_2\text{Cl}_2$  + TFA,  $\lambda_{\text{exc}} = 330$  nm. (c)  $\text{CH}_2\text{Cl}_2$  + TFA,  $\lambda_{\text{exc}} = 360$  nm.

is observed simultaneously with a relative increase in the yield of the CT emission at 504 nm, by excitation at 330 nm. Only the CT emission is observed at long exciting wavelengths, however (see Figure 4).

**Photochemistry.** Our preliminary studies on the photochemical behavior of **1g**, which was found to yield the efficient intramolecular hydroxylation products **3g** and **3g'** (Table 2), revealed<sup>13</sup> oxygen-free 0.1 mM  $\text{CH}_2\text{Cl}_2$  solutions of **1g** containing 0.1 M TFA to provide good results. These conditions provide very clean reaction mixtures and high yields of intramolecular hydroxylated materials, with minimal yields in deoxygenated **2g** and quenching of the rearrangement processes.<sup>22</sup> Irradiation (Pyrex filter) of **1a–f** under the same conditions (Scheme 3) yielded the corresponding deoxygenated **2a–g** and the parent hydroxylated **3a–g** compounds. The structure of the hydroxylated products **3a–g** was determined by <sup>1</sup>H

### SCHEME 3. Photoproducts of the *N*-Oxides **1a–g**



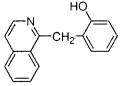
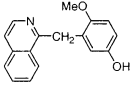
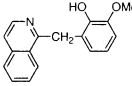
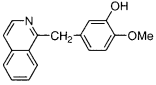
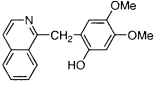
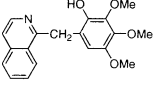
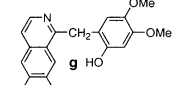
and <sup>13</sup>C NMR spectroscopy and from mass spectra, as well as by comparison with authentic samples in some cases. The yields of the preparative photoreactions are listed in Table 2. Except for **1d**, the yields for the hydroxylated compounds (**3a–g**) exceeded those for the deoxygenated products (**2a–g**).

The photolysis of **1a** gave the deoxygenated precursor **2a**, with the regioisomer **3a** as the sole hydroxylated material. Their spectroscopic data and a comparison with an authentic sample<sup>5</sup> allowed us to unequivocally assign their structure. Although the clear reaction mixture was carefully analyzed, no other hydroxylated regioisomer was detected.

The photolysis of the mono-methoxylated compounds **1b–d** provided interesting results. Thus, irradiation of the *o*- and *m*-methoxy compounds **1b,c** produces two sets of regioisomeric hydroxylated compounds (**3b, 3b'** and **3c, 3c'**) in addition to the corresponding deoxygenated compounds (**2b,c**). Also, the photoreaction of **1d** again gave the derivative **3d** as the sole hydroxylated material. The presence of the hydroxy group farther away than the ortho position with respect to the methylene bridge in the aryl donor (as in structures of **3b, 3b'**, and **3d**) was a singular result. The interpretation of the spectroscopic data allowed us to assign the position for the ring hydroxylation. Because of the mechanistic implications, these remarkable results had to be unambiguously veri-

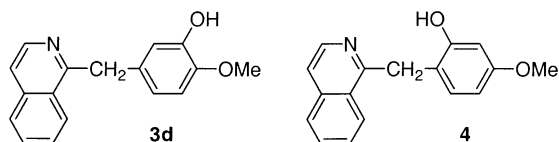
(22) Bremmer, J. B.; Wiriyachitra, P. *Aust. J. Chem.* **1973**, *26*, 437–442.

**TABLE 2.** Yields (%)<sup>a</sup> of the Photoproducts from the Irradiation of **1a–g** in Degassed CH<sub>2</sub>Cl<sub>2</sub>/0.1 M TFA Solutions

Entry	Photoproduct		Conversion %
	2	3	
<b>a</b>	16	 <b>a</b> :57	92
<b>b</b>	18	 <b>b</b> :26	<b>b'</b> :17 55 <sup>b</sup> 83
<b>c</b>	7	 <b>c</b> :12	<b>c'</b> :41 53 <sup>b</sup> 85
<b>d</b>	67	 <b>d</b> :14	91
<b>e</b>	31	 <b>e</b> :31	<b>e'</b> :10 41 <sup>b</sup> 89
<b>f</b>	33	 <b>f</b> :41	75
<b>g</b> <sup>c</sup>	23	 <b>g</b> :73	<b>g'</b> :2 75 <sup>b</sup>

<sup>a</sup> Calculated on the basis of consumed *N*-oxides. <sup>b</sup> Overall photohydroxylation yields. <sup>c</sup> Data from ref 13.

fied, by comparison with both possible regioisomers (**3d** and **4**), which were synthesized as shown in Scheme 2. A comparison of the physical and spectroscopic data allowed us to unequivocally establish the structure of **3d** as the hydroxylated material derived from this photochemical reaction.



On the basis of our previous results for the photochemistry of **1g**, the photolysis of **1e** gave the expected regioisomeric mixture of hydroxylated compounds (**3e** and **3e'**). These compound possess the same dimethoxybenzene moiety as donor unit as the previously studied **1g**; likewise, the two expected hydroxylated compounds, ortho to the methylene bridge, were detected, albeit in a more even proportion (with the former in a higher yield).

As expected, the photolysis of the trimethoxylated compound **1f** gave the only possible photohydroxylation product **3f**. In fact, **3f** contains a highly functionalized aromatic ring (four consecutive oxygenated and one alkyl substituent), which is consistent with the efficient hydroxylation despite the steric hindrance and electronic factors on the aromatic ring.

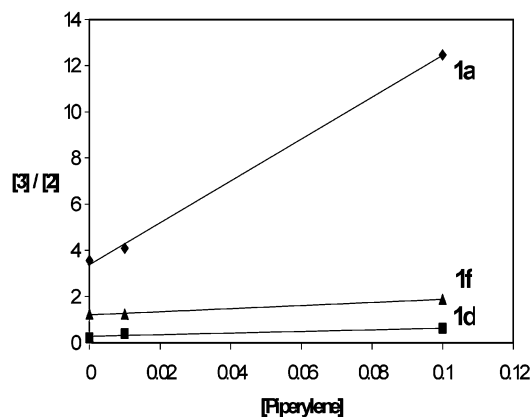
**Quenching and Sensitization Experiments.** As stated above, there seems to be general agreement that

the photochemical deoxygenation of *N*-oxides originates from the triplet state. However, the hypotheses that both reactions involve the singlet state and the same intermediate (an oxaziridine), which can both transfer an oxygen atom to the medium and rearrange further, have often been presented. Direct experimental support, such as that provided by sensitization or quenching experiments, is scant. To gain insight into the mechanism of the hydroxylation process, it is therefore necessary to determine the nature of the excited states involved in the photochemical reaction leading to the formation of the resulting compounds.

**Quenching of T<sub>1</sub> by Piperylene.** The involvement of two different excited states in the photochemical pathway has been shown by comparing the results of the photoreaction in the absence and presence of an isoquinoline *N*-oxide triplet quencher. The triplet excitation energy<sup>23</sup> for isoquinoline *N*-oxide was determined from the phosphorescence maximum to be about 53.7 kcal mol<sup>-1</sup>; by contrast, that for the protonated form<sup>13</sup> is 61.6 kcal mol<sup>-1</sup>. In this work, we examined the photochemical implications of the presence of piperylene (*E*<sub>T</sub> = 59 kcal mol<sup>-1</sup>),<sup>24</sup> a commonplace triplet quencher that cannot act as a triplet photosensitizer because of its poor absorption characteristics and short lifetime.

(23) Ono, I.; Hata, N. *Bull. Chem. Soc. Jpn.* **1973**, *46*, 3658–3662.

(24) Turro, N. J. *Modern Molecular Photochemistry*; University Science Books; Mill Valley, CA, 1991.



**FIGURE 6.** Variation of the  $[3]/[2]$  ratio with the piperylene concentration.

**TABLE 3.** Ratio of Photohydroxylation to Photodeoxygenation ( $[3]/[2]$ ) in the Photolysis of **1a,d,f** at Different Piperylene Concentrations

	[piperylene]		
	0	0.01	0.1
<b>1a</b>	3.6	4.1	12.5
<b>1d</b>	0.2	0.4	0.6
<b>1f</b>	1.2	1.2	1.9

**TABLE 4.** Photodeoxygenation (**2a**) and Photohydroxylation (**3a**) Yields in the Photolysis of **1a** in the Presence of Benzophenone as Sensitizer

[benzophenone]	photoproducts	
	<b>2a</b>	<b>3a</b>
0.0	16	57
0.1	80	0

For simplicity in the analysis of the reaction mixture, we only examined the photolysis of **1a**, **1d**, and **1f** since they yielded only two photoreaction products, namely the corresponding photodeoxygenated derivatives (**2a**, **2d**, and **2f**), and a single photohydroxylation derivative (**3a**, **3d**, and **3f**, respectively). Furthermore, these three compounds span the range of redox properties of the studied compounds (**1a–f**). Table 3 and Figure 6 show the yields obtained in the quenching experiments. With **1a**, the  $3a/2a$  ratio in the absence of quencher was 3.6. The photodeoxygenation leading to the formation of **2a** was effectively quenched by the presence of piperylene, and the photohydroxylation increased by a factor of almost 4 by increasing the quencher concentration to 0.1 M. This was reflected in an increase in the  $3a/2a$  ratio to 12.5. With **1d** and **1f** as the substrates, quenching was less marked, as reflected in the decreased slopes of the plots (Figure 6). These results clearly suggest that isoquinoline *N*-oxide photodeoxygenation is efficiently quenched by piperylene and that it originates from the triplet-excited state.

**Triplet Photosensitization.** A sensitization experiment was conducted to clarify the origin of the deoxygenation and hydroxylation. **1a** photolyzates were analyzed in the presence and absence of benzophenone ( $E_T = 69 \text{ kcal mol}^{-1}$ ).<sup>24</sup> The results obtained are summarized in Table 4.

The dependence of the photoreaction pathway on the presence of the sensitizer resulted in a dramatic difference in the outcome of the reaction. Benzophenone inhibited the formation of the hydroxylated compound **3a** and raised the yield in **2a**. Hence, the only photoprocess observed was deoxygenation as the excited state that gave rise to **3a** could not be reached by direct triplet sensitization. Consequently, the hydroxylation must arise from an excited state that cannot be reached from the isoquinoline *N*-oxide  $T_1$  state.

## Discussion

The photochemical results obtained in this work (Table 2) provide unequivocal evidence that both deoxygenation to **2a–f** and hydroxylation to **3a–f** are the general pathways upon photoexcitation of acid solutions of the *N*-oxides **1a–f**. The most significant difference in the photochemical consequences is the ratio of deoxygenation (**2**) to hydroxylation (**3**) material obtained. Because all the **1a–f** *N*-oxides possess the same acceptor unit (the protonated form of the isoquinoline *N*-oxide), the difference should be attributed mainly to the mono-electronic oxidative ability of each donor moiety. In this respect, the synthesis of this series of  $A^+–S–D$  systems (**1a–f**) has proved useful for elucidating the mechanistic implications on the photophysical and photochemical behavior.

**Photophysics.** The studied systems contain two chromophores that are covalently connected but not conjugated; also, their absorption spectra are simply the combination of those for the isolated chromophores (Figure 2). Obviously, these compounds experience no extensive electronic interaction between the constituting chromophores. Also, it should be noted that the intramolecular acceptor/donor separation is not too large, and that the 2-nm bathochromic shift observed with respect to the individual elements in the  $A^+–S–D$  systems indicates further, but insubstantial stabilization in the ground state. The donor chromophores incorporated into these bichromophoric molecules exhibit negligible absorption up to 300 nm, whereas the acceptor chromophore exhibits strong absorption in the 240–280- and 290–320-nm regions. As a result, the absorption spectra for all the studied compounds are largely dominated by the contribution of the isoquinoline *N*-oxide moiety and the changes due to the presence of the different studied donors cannot be fully observed.

Clearly, the situation is rather different in regard to the electronic emission spectra. The donor chromophores in the  $A^+–S–D$  systems are nonfluorescent, presumably as a result of extremely rapid radiationless relaxation under concomitant energy transfer to the emissive  $S_1$  state of the acceptor. Under neutral conditions, the LE emission due to the *N*-oxide chromophore prevails (Figure 3 is quite consistent with this situation for compounds **1a–e**, for which only the nonstructured band at 394 nm is obtained, whichever the excitation wavelength chosen). As derived from the Weller equation<sup>25</sup> for isoquinoline *N*-oxide systems,<sup>13</sup> there is no driving force for the electron transfer in **1a–e**; also, no other fluorescent excited state can be reached by these bichromophoric systems. In comparing the data, attention should be given

(25) Rehm D.; Weller, A. *Isr. J. Chem.* **1970**, *8*, 259–271.

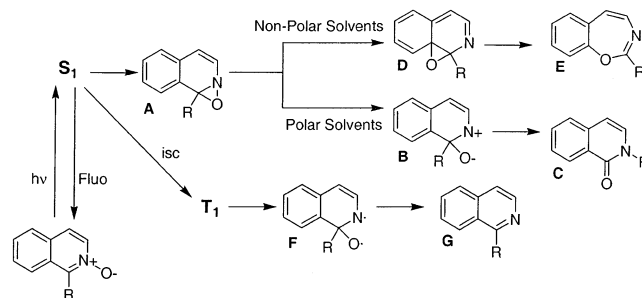
to the effect of the medium as the observed reduction potentials with *N*-oxides are pH-dependent, so their reduction is easier under acid conditions.<sup>7</sup> Thus, on protonation of the oxygen atom of the *N*-oxide function, reduction by one-electron transfer from the donor ground state to the acceptor excited state is indeed possible and an emissive CT state can be reached.

Compound **1f** exhibits a special feature: it exhibits the dual fluorescence emissions in both neutral and acid solutions. In the latter, however, relative intensities are increased with respect to the CT emission. Even in neutral environments, the emission from the CT state reveals that the electron transfer operates effectively in this redox system. As can be inferred from the Rehm–Weller equation,<sup>25</sup> the reduction potential of the acceptor is less favorable under neutral conditions (the  $\Delta G$  factor thus being less favorable), but this can be offset by the decreased reduction potential of the trimethoxylated donor.

The emissive contours of the protonated species **1a–e** in dichloromethane solutions are very strongly dependent on the excitation wavelength. With excitation at short wavelengths ( $\lambda_{\text{exc}}$  330 nm), only the LE emission of the protonated isoquinoline *N*-oxide was observed at ~382 nm, blue shifted with respect to the neutral chromophore. However, the appearance of a new red-shifted emission band up to 400 nm, when using long-wavelength light, reveals that an emissive CT state was reached. The detectability of such CT fluorescence is further enhanced by its significant Stokes shift, which tends to move it into a region not overlapped by the residual LE emission of the acceptor. The fluorescence data of Table 1 are shown graphically in Figure 4. All the compounds from **1a** to **1f** behave as dual-channel fluorescent systems. The LE emission always remains at the same emission wavelength, which is consistent with the fact that all possess the same chromophoric acceptor, i.e., the protonated form of the isoquinoline *N*-oxide. However, the long-wavelength emission band shifts from 449 nm for **1a** to 512 nm for **1f**. This bathochromic shift is correlated with the increased donor ability of the donor moiety in the **1a–f** series. The increase in the Stokes shift with decreasing oxidation potential of the donor reflects the decrease in energy of the corresponding CT states. The change in Gibbs free energy ( $\Delta G$ ) between the initial ( $S_1$ ) and final state (CT) is a crucial parameter in all discussions concerning electron-transfer processes.<sup>1</sup> The comparisons of LE and CT intensities for the emission bands in Figure 4 clearly show that the relative ease with which the CT state can be populated correlates well with the simultaneous depopulation of the LE state. This reflects the fact that the electron transfer operates as an efficient pathway for depopulating the  $S_1$  state of the protonated form of the isoquinoline *N*-oxide by decreasing the reduction potential of the donor.

From the data in Table 1 and Figure 4 it clearly follows that extensive or even complete quenching of the acceptor fluorescence occurs in all the systems studied (**1a–f**). Intramolecular electron transfer is assumed to provide the additional decay channel responsible for this quenching. The occurrence of intramolecular electron transfer as a quenching mechanism is unequivocally supported by the appearance of a long-wavelength fluorescence that can be ascribed to radiative deactivation of the CT state

#### SCHEME 4. Proposed Photochemical Reactivity for Heterocyclic Aromatic *N*-Oxides



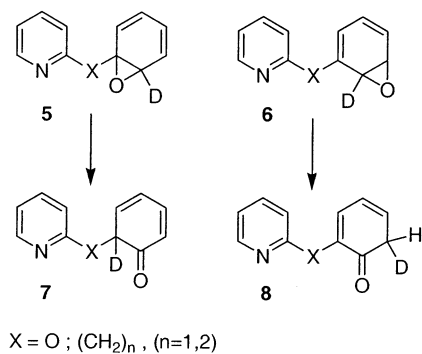
populated upon the electron transfer. One common feature of dual-channel fluorescent chemosensors is that substrate binding enhances one emission channel at the expense of the other. Our results constitute an exception to this generalization as the combination of two signaling mechanisms (*N*-oxide oxygen binding to chemical species and induction of electron transfer) allows two fluorescent emission bands to be obtained. Compounds **1a–e** exhibit both quenching in the LE emission of the isoquinoline *N*-oxide and the simultaneous appearance of two independent emission bands at short and long wavelengths. From the logic viewpoint, the output can be high when either protons or other cationic species are bound to the *N*-oxide function and precise selection of the excitation wavelength results in the independent appearance of the two emitting channels. One specially significant feature is the (apparent) absence of interaction of both emitting channels.

On the other hand, compound **1f** results in a photoionic logic system in which both short- and long-wavelength emission bands occur simultaneously at high excitation energies, and only the long-wavelength emission bands remain at less energetic excitations.

Although molecules **1a–f** provide a rudimentary foundation for future molecular photoionic devices, preliminary applications such as fluorosensors by incorporation into new chemical guest systems<sup>5</sup> have proved to be a promising approach to the development of photochemical systems and materials that can respond in a controllable manner to chemical and/or optical stimuli.

**Photochemistry.** Interestingly, the studied compounds exhibit efficient photochemical reactions (deoxygenation and aromatic hydroxylation) that yield two main products, namely, the parent aromatic amines **2a–f** and the phenolic derivatives **3a–f**, respectively (Scheme 3).

The photochemical reactions of heteroaromatic amine *N*-oxides have been the subject of a number of publications<sup>7,8</sup> from which it has been established that, upon excitation to the  $S_1$  excited state, their photochemistry arises, formally, from the rearrangement of oxaziridine (A) leading to ring expansion, ring contraction, and further oxygen migration around the heterocyclic nucleus (Scheme 4).<sup>12</sup> One attractive, plausible mechanistic interpretation of the behavior of alkyl-substituted heterocyclic *N*-oxides assumes that, in polar solvents, the next step involves the formation of the zwitterions (B), followed by a [1,2] shift of the R group to achieve the isoquinolone (C). In nonpolar solvents, the pathway from the oxaziridine is formulated as a [1,5] sigmatropic shift to the epoxy structure (D), followed by a new [1,5] shift

**SCHEME 5. Intermediates Considered in the Intramolecular Aromatic Hydroxylation via Irradiation of Pyridine *N*-Oxide Derivatives**


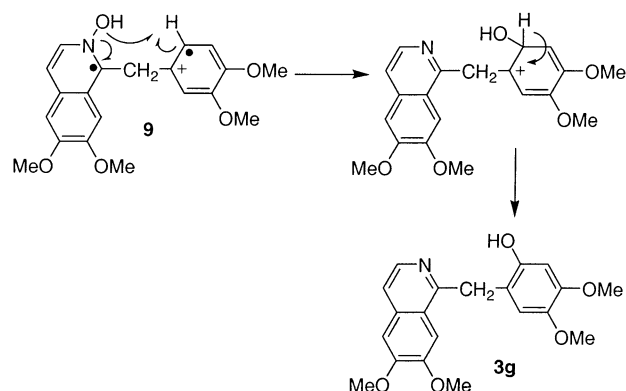
to the oxazepine (E). In competition with the rearrangement reactions, S<sub>1</sub> to T<sub>1</sub> intersystem crossing as been proposed as the pathway leading to a triplet biradical (F). This has been claimed as the mechanism responsible for the photochemical deoxygenation via oxygen transfer from the *N*-oxide group to various substrates.

Despite these general statements, some authors have failed to observe a potential oxaziridine intermediate.<sup>26</sup> Experimental evidence suggests that the excited singlet state is the last species common to the photoproducts C and E. Whatever the mechanism may be, the rate of isoquinolone formation is largely independent of the solvent, so the solvent effect must be ascribed to a change in the rate of oxazepine formation.

Kinetic studies<sup>15b</sup> of atomic oxygen in solution with laser flash photolysis of pyridine *N*-oxide point to a mechanism in which the solvent reacts with an *invisible* species (atomic oxygen) to yield the observed transients. Rapid release of <sup>3</sup>O from the *N*-oxide functional group in the lowest excited singlet state (S<sub>1</sub>) has also been considered for pyridine *N*-oxide.<sup>9,15b</sup> These studies support the formation of oxygen atom (accompanied by other intramolecular processes, however); also, a number of questions concerning these reactions still remain open.

Because the rearrangement product results mainly from the oxaziridine (A), methods for suppressing this photochemical pathway, by complexation, have been developed. Several authors<sup>12,27</sup> found the photochemical behavior of heteroaromatic *N*-oxides to always be less complicated, and high yields of the deoxygenated bases to be obtained, in the presence of Lewis acids. The Lewis acid is thought to bind the nucleophilic oxygen, thereby inhibiting the undesirable rearrangement to oxaziridine and its congeners. The photolysis of these complexes can yield phenols, both in an inter- and in an intramolecular way, via a NIH mechanism. However, on the basis of these results (see Scheme 5), the reaction proceeds via an oxenoid mechanism (i.e. the transfer of atomic oxygen) that leads to either or both of the arene oxides **5** and **6**; these in turn can rearrange to the cyclohexanedienones **7** and **8**. While intermediate **7** can only aromatize with loss of deuterium, **8** can lose either a proton or a deuterium atom and give rise to the NIH shift.

In previous studies<sup>13</sup> on the photochemistry of **1g**, we proposed (Scheme 6) that, after fast electron transfer

**SCHEME 6. Concerted Mechanism Proposed for the Photochemical Hydroxylation of Papaverine *N*-Oxide**


from the donor moiety to the singlet excited state of the protonated form of the acceptor *N*-oxide, the fate of the CT state **9**, which is a diradical ion pair, is the homolytic rupture of the N–O bond to transfer the hydroxyl radical to the benzene ring. Proton losses upon rearomatization yield the intramolecular hydroxylation product.

The results for the photochemistry of *N*-oxides **1a–f** in acid solutions allowed us to verify that the hydroxylation of the aromatic donor moiety leading to **3a–f** is a common result for these compounds, which are accompanied by variable amounts of the parent deoxygenated substances (**2a–f**). Interestingly, these systems can undergo a single-electron-transfer reaction that results in bond-cleavage/bond-construction with a regioselective stipulation.

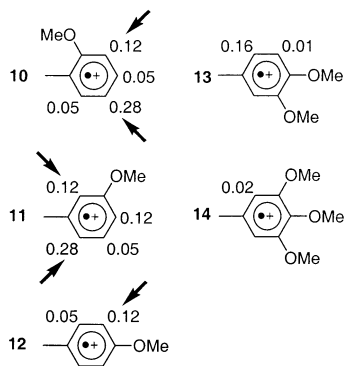
The detection of the hydroxylated compounds **3a–f** having the hydroxy function at specific positions of the aromatic moiety, and the comparative analysis of the different models of substitution, clearly reveals strict requirements for the bond-construction step. This has two major implications. First, the hydroxylation site is not restricted to the ortho position with respect to the methylene bridge. The two hydroxylated derivatives (**3g** and **3g'**) previously reported,<sup>13</sup> as well as the new ones (**3a**, **3c**, **3c'**, **3e**, **3e'**, and **3f**) described herein, can be justified in terms of an intermediate such as **9** (Scheme 6). Consequently, the N–O bond cleavage cannot exclude a simultaneous Ar–O bond construction, in a concerted process, via a reasonable six-member intermediate. Other concerted intermediates have been proposed for quinoxaline<sup>28</sup> and pteridine<sup>29</sup> *N*-oxide derivatives. However, because **3b**, **3b'**, and **3d** have the hydroxylation site in a remote position (meta or para to the methylene bridge), they clearly exclude the concerted process and point to a sequential bond-cleavage/bond-construction mechanism. Second, the hydroxylation sites in the cation-radical that derives from the donor moiety after the electron transfer is consistent with the spin densities reported for the model compounds, as shown in Scheme 7. Spin densities based on Huckel calculations for some methoxy-substi-

(28) Kurasawa, Y.; Takada, A.; Kim, H. S. *J. Heterocycl. Chem.* **1995**, *32*, 1085–1114.

(29) (a) Sako, M.; Shimada, K.; Hirota, K.; Maki, Y. *Tetrahedron Lett.* **1985**, *26*, 6493–6496. (b) Sako, M.; Ohara, S.; Hirota, K.; Maki, Y. *J. Chem. Soc., Perkin Trans. 1* **1990**, 3339–3344.

(26) Lohse, C. J. *Chem. Soc., Perkin Trans. 2* **1972**, 229–233.

(27) Hata, N.; Ono, I.; Kawasaki, M. *Chem. Lett.* **1975**, 25–28.

**SCHEME 7. Spin Densities for Methoxybenzene Radical Cations<sup>a</sup>**


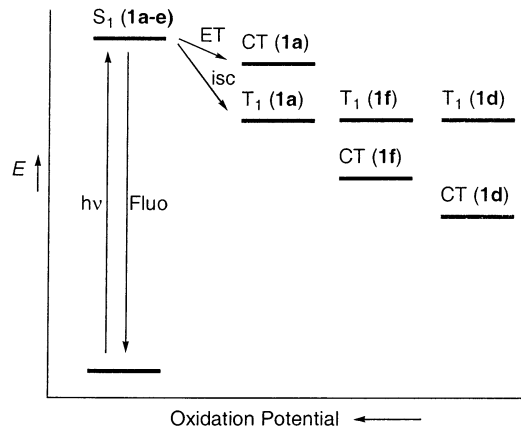
<sup>a</sup> Arrows denote reported hydroxylation positions in the parent compounds **1b–d**.

tuted benzenes are shown in Scheme 7.<sup>30</sup> Both charge<sup>31</sup> and spin densities<sup>32</sup> have been widely discussed in relation to  $S_N2Ar^*$  and radical processes in the literature. The directing influence of the electron-donor substituents can be rationalized in terms of the calculated values for cation-radicals.

A comparison of Scheme 7 with the reaction data in Table 2 reveals significant correlation. The high spin density positions in **10** are consistent with the observed hydroxylation selectivity. Compounds **3b** and **3b'** correspond to hydroxylation positions that agree with the two high spin densities (0.28 and 0.12) in **10**. Interestingly, the high yield for **3b** relative to **3b'** corresponds to the high spin density position. *N*-oxide **1c** gives both the **3c** and the **3c'** phenol, which is also consistent with two high spin density positions in cation-radical **11**. The possibility of reacting with two positions ortho to the methylene bridge instead of with the para position may account for the fact that no *p*-hydroxy-compound was detected, consistent with the energy balance for the solvent reorganization needed to achieve the para position. Again, the high yield of the photoproduct **3c'** relative to **3c** exposes a relationship with the highest spin density of 0.28 in cation-radical **11**. Similarly, the hydroxylated-only material **3d** that derives from **1d** has the hydroxyl function in the meta position (i.e. the highest spin density on cation-radical **12**).

The results obtained in the photolysis of **1e** and **1g**, both of which have the same substituents in the donor moiety, can be rationalized in terms of the high spin density of the resulting cation-radical (**13**) in the ortho position relative to the others. The relatively low yield of **3f** (the system having the best donor and the ortho position as the sole reactive site) can be rationalized in terms of the resulting low spin density (0.02) of the parent cation-radical (**14**).

**Excited States Involved in the Photochemical Process.** As noted earlier, the lowest triplet state for aromatic amine *N*-oxides is usually regarded as the

**SCHEME 8. Generalized Energy Level Diagram for Bichromophoric A<sup>+</sup>–S–D Systems**


reactive intermediate responsible of the photochemical deoxygenation to the parent amines. With this premise in mind, but taking into account that the two-step (bond-cleavage/bond-construction) process leading to hydroxylation can be interrupted if bond cleavage is followed by hydroxy-radical migration and some deoxygenation material can be formed via this disruptive pathway as a result, the question arises as to which excited state drift affects each photoproduct. To approach this question, we carried out the quenching and sensitization experiments described above.

Pyperilene was found to effectively quench the triplet involved in the photoreaction and to reduce the production of deoxygenated material (Table 3). This effect was more marked on **1a** but still appreciable on **1d** and **1f** (Figure 6); it suggests that the triplet state of the protonated isoquinoline *N*-oxide persists as that responsible for the deoxygenation path. Clearly, the photosensitization of **1a** with benzophenone reveals that their triplet state deoxygenates efficiently and that the hydroxylation material comes from another state that cannot be reached from this one.

If we assume all protonated *N*-oxides **1a–e** have the same acceptor moiety, locating their triplet state at the same energy level, and that decreasing the donor reduction potential produces CT states with a gradually decreasing energy as can be inferred from their wavelength emissions, then the CT state of **1a** must be the only one with a higher energy than the  $T_1$  state. Therefore, the quenching of intersystem crossing to its  $T_1$  state should result in a higher [**3a**]/[**2a**] ratio.

In summary, on the basis of the body of data reported here, we can consider (Scheme 9) three main pathways for the depopulation of the  $S_1$  excited state in the  $A^+–S–D$  systems studied, namely, LE fluorescence emission, intersystem crossing to the  $T_1$  state, and electron transfer to a CT state. All three are effective and depopulate  $S_1$  efficiently, since the described products characteristic of their reactivity<sup>33</sup> are not detected. The photoreaction of **1a–f** yields two products only: photodeoxygenated and photohydroxylated materials. Intersystem crossing to  $T_1$  is the main pathway to the photodeoxygenated material. In competition, electron transfer from the donor moiety

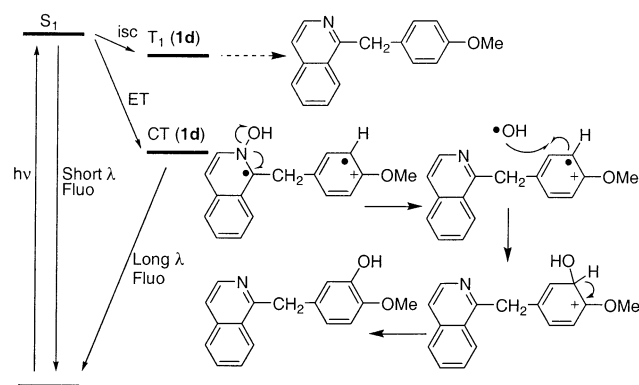
(30) (a) Zweig, A.; Hodgson, W. G.; Jura, W. H. *J. Am. Chem. Soc.* **1964**, *86*, 4124–4129. (b) Sunberg, R. J. In *Organic Photochemistry*; Padwa, A., Ed.; Marcel Dekker, Inc.: New York, 1983; Vol. 6.

(31) Gilbert, A.; Baggott, J., Eds. *Essentials of Molecular Photochemistry*; Blackwell Scientific Publications: Oxford, UK, 1991.

(32) Said, A. H.; Mhalla, F. M.; Amatore, C.; Verpeaux, J.-N. *J. Electroanal. Chem.* **1999**, *464*, 85–92.

(33) Bremner, J. B.; Wiryachitra, P. *Aust. J. Chem.* **1973**, *26*, 437–442.

**SCHEME 9. Proposed Mechanism for the Photochemical Behavior of the A<sup>+</sup>–S–D Systems, Illustrated for 1d**



to the  $S_1$  excited state of the acceptor leads to an emissive CT state that is responsible for the hydroxylated products. The CT state undergoes a homolytic N–O bond scission to give the hydroxy radical and a cation-radical pair. The cleavage, which may occur when the electron transfer takes place, restores the isoquinoline nucleus and gives the radical/cation-radical pairs as transient intermediates. Bond formation by coupling of the hydroxyl radical and the aryl cation-radical is a radical process that is regioselectively controlled by the spin densities of the resulting donor cation-radicals. Proton losses to restore aromaticity give the hydroxylated products.

### Conclusions

The A<sup>+</sup>–S–D bichromophoric systems studied were found to be dual-channel fluorescent compounds where both LE and CT emissions can be modulated simply by modifying the donor ability. Judicious design and synthesis of these structures can provide attractive sensors that combine and compete between photoluminescence and photoinduced electron transfer. These sensors are of special significance on account of their potential biological applications; in fact, compounds **1a–f** are closely related to natural isoquinoline alkaloids, for which some receptors have been reported.<sup>34</sup>

Deoxygenation to the parent amine and hydroxylation of the aromatic donor moiety were found to be the sole photochemical processes involved. The aromatic photohydroxylation is a radical process that is regioselectively guided by the residual spin density of the resulting cation-radical, a process that is initiated by an intramolecular electron transfer. The proposed mechanism provides a rational basis for our photochemical results and also an approach to the interpretation of the controversial oxygen walk process.<sup>12</sup>

### Experimental Section

**Material and Equipment.** All starting material and reagents were used as received. Solvents were spectrophotometric or HPLC grade and were used without further purification. HRMS are reported as *m/z*. Accurate masses are reported for the molecular ion ( $M + 1$ ). <sup>1</sup>H and <sup>13</sup>C NMR spectra (200

and 50 MHz, respectively) were recorded from CDCl<sub>3</sub> solutions, using the solvent residual proton signal as standard. TLC analyses were performed on silica gel 60 F 256 plates and column chromatography was carried out on silica gel 60 (70–230 mesh). Melting points were obtained in open capillaries and are uncorrected.

**Spectroscopic Studies.** Samples for UV/Vis and emission spectra were prepared in spectroscopic grade solvents and adjusted to linear range response. Molar absorption coefficients were determined by using concentrations of 10<sup>−4</sup> or 10<sup>−5</sup> M. No fluorescent contaminants were detected upon excitation in the wavelength region of experimental interest. Fluorescence quantum yields were determined by comparison with 0.1 M quinine sulfate in 0.05 M sulfuric acid as reference, and corrected for the refractive index of the solvent. The samples were made with an absorbance between 0.1 and 0.2 at the excitation wavelength. 3D fluorescence spectra were recorded by increasing the excitation wavelength for 1 nm.

**General Procedure for Irradiation of Samples 1a–f.** Photolyses were performed under an argon atmosphere. An immersion well photoreactor (Pyrex) equipped with a medium-pressure mercury lamp (150 W) was used. Magnetically stirred solutions (10<sup>−3</sup> M) of the corresponding *N*-oxides in 0.1 M TFA in CH<sub>2</sub>Cl<sub>2</sub> were irradiated for 6 or 10 min. The photolysates were washed with aqueous NaHCO<sub>3</sub> and H<sub>2</sub>O, and dried over MgSO<sub>4</sub>. The solvent was evaporated under reduced pressure, and the resulting material was dissolved in the minimal amount of chloroform and subjected to column chromatography with hexane/ethyl acetate (from 4:1 to 1:1). The respective photodeoxygenated products obtained (**2a–f**) were identified by comparison with the synthesized samples (see Supporting Information). When necessary, mixtures of regioisomeric phenols were further separated by preparative TLC with (47:3) chloroform/methanol.

**1-(2-Hydroxybenzyl)isoquinoline (3a).** See ref 5.

**1-(2-Methoxy-5-hydroxybenzyl)isoquinoline (3b).** Brown oil; <sup>1</sup>H NMR (200 MHz, CDCl<sub>3</sub>) δ 3.86 (s, 3H), 4.52 (s, 2H), 6.63 (d, 1H, *J* = 2.4 Hz), 6.76 (dd, 1H, *J* = 3.0, 8.5 Hz), 6.76 (d, 1H, *J* = 8.5 Hz), 7.17 (d, 1H, *J* = 5.5 Hz), 7.51 (dt, 1H, *J* = 1.2, 8.2 Hz), 7.65–7.77 (m, 2H), 7.78 (d, 1H, *J* = 7.9 Hz), 8.05 (d, 1H, *J* = 7.9 Hz); <sup>13</sup>C NMR (50 MHz, CDCl<sub>3</sub>) δ 34.1, 56.3, 112.2, 114.1, 116.5, 120.3, 126.6, 126.9, 127.2, 127.6, 128.3, 130.6, 136.5, 139.5, 149.5, 151.5, 160.8; MS *m/z* (%) 265 (1) [ $M$ ]<sup>+</sup>, 234 (100), 84 (44); HRMS (FAB) *m/z* calcd. for C<sub>17</sub>H<sub>15</sub>NO<sub>2</sub> (M)<sup>+</sup> 265.1103, found 265.1097.

**1-(2-Methoxy-3-hydroxybenzyl)isoquinoline (3b').** Brown oil; <sup>1</sup>H NMR (200 MHz, CDCl<sub>3</sub>) δ 3.87 (s, 3H), 4.68 (s, 2H), 6.49 (t, 1H, *J* = 4.3 Hz), 6.77 (d, 2H, *J* = 5.5 Hz), 7.46–7.66 (m, 3H), 7.79 (d, 1H, *J* = 7.3 Hz), 8.10 (d, 1H, *J* = 8.5 Hz), 8.46 (d, 1H, *J* = 6.0 Hz); <sup>13</sup>C NMR (50 MHz, CDCl<sub>3</sub>) δ 36.6, 55.8, 112.9, 116.3, 118.7, 120.3, 122.8, 125.2, 126.0, 127.6, 127.9, 130.8, 136.9, 139.9, 150.9, 152.9, 160.9; MS *m/z* (%) 265 (4) [ $M$ ]<sup>+</sup>, 234 (100); HRMS (FAB) *m/z* calcd. for C<sub>17</sub>H<sub>15</sub>NO<sub>2</sub> (M)<sup>+</sup> 265.1103, found 265.1091.

**1-(2-Hydroxy-5-methoxybenzyl)isoquinoline (3c).** Pale yellow solid; mp 139–142 °C; <sup>1</sup>H NMR (200 MHz, CDCl<sub>3</sub>) δ 3.73 (s, 3H), 4.54 (s, 2H), 6.68 (dd, 1H, *J* = 1.2, 5.8 Hz), 6.68–6.92 (m, 2H), 7.56 (d, 1H, *J* = 5.5 Hz), 7.68–7.84 (m, 3H), 8.34 (d, 1H, *J* = 5.5 Hz), 8.41 (d, 1H, *J* = 9 Hz); <sup>13</sup>C NMR (50 MHz, CDCl<sub>3</sub>) δ 36.1, 55.9, 110.5, 119.4, 120.2, 122.1, 125.5, 126.4, 127.6, 127.8, 130.8, 136.9, 139.9, 145.9, 149.4, 160.9; MS *m/z* (%) 265 (100) [ $M$ ]<sup>+</sup>, 248 (69); HRMS (FAB) *m/z* calcd. for C<sub>17</sub>H<sub>15</sub>NO<sub>2</sub> (M)<sup>+</sup> 265.1103, found 265.1106.

**1-(2-Hydroxy-3-methoxybenzyl)isoquinoline (3c').** Pale yellow solid; mp 129–131 °C; <sup>1</sup>H NMR (200 MHz, CDCl<sub>3</sub>) δ 3.85 (s, 3H), 4.60 (s, 2H), 6.72–6.75 (m, 2H), 6.88 (t, 1H, *J* = 4.8 Hz), 7.54 (d, 1H, *J* = 5.5 Hz), 7.61–7.73 (m, 2H), 7.81 (d, 1H, *J* = 5.5 Hz), 8.33–8.42 (m, 2H); <sup>13</sup>C NMR (50 MHz, CDCl<sub>3</sub>) δ 35.3, 61.4, 114.1, 120.0, 121.5, 124.7, 124.9, 125.9, 127.3, 127.4, 130.1, 132.6, 136.5, 141.5, 144.7, 149.1, 159.9; MS *m/z* (%) 265 (43) [ $M$ ]<sup>+</sup>, 248 (100); HRMS (FAB) *m/z* calcd. for C<sub>17</sub>H<sub>15</sub>NO<sub>2</sub> (M)<sup>+</sup> 265.1103, found 265.1093.

(34) Benavides, J.; Quateronet, D. *J. Neurochem.* **1983**, *41*, 1744–1750.

**1-(3-Hydroxy-4-methoxybenzyl)isoquinoline (3d).** Pale yellow solid; mp 165–167 °C;  $^1\text{H}$  NMR (200 MHz,  $\text{CDCl}_3$ )  $\delta$  3.79 (s, 3H), 4.56 (s, 2H), 6.72–6.78 (m, 3H), 7.46–7.53 (m, 2H), 7.62 (dt, 1H,  $J = 1.2, 5.5$  Hz), 7.78 (d, 1H,  $J = 7.9$  Hz), 8.13 (d, 1H,  $J = 8.5$  Hz), 8.40 (d, 1H,  $J = 5.5$  Hz);  $^{13}\text{C}$  NMR (50 MHz,  $\text{CDCl}_3$ )  $\delta$  41.0, 55.9, 109.9, 110.8, 114.9, 116.5, 119.8, 120.0, 122.2, 124.8, 126.0, 127.3, 127.4, 130.2, 130.7, 132.4, 136.7, 141.1, 145.2, 145.7, 160.2; MS  $m/z$  (%) 265 (62)  $[M]^+$ , 264 (100); HRMS (FAB)  $m/z$  calcd for  $\text{C}_{17}\text{H}_{15}\text{NO}_2$  (M) $^+$  265.1103, found 265.1115.

**1-(2-Hydroxy-4,5-dimethoxybenzyl)isoquinoline (3e).** Colorless oil;  $^1\text{H}$  NMR (200 MHz,  $\text{CDCl}_3$ )  $\delta$  3.79 (s, 3H), 3.80 (s, 3H), 4.49 (s, 2H), 6.58 (s, 1H), 6.80 (s, 1H), 7.55 (d, 1H,  $J = 5.5$  Hz), 7.67–7.85 (m, 3H), 8.33 (d, 1H,  $J = 5.5$  Hz), 8.41 (d, 1H,  $J = 8.3$  Hz);  $^{13}\text{C}$  NMR (50 MHz,  $\text{CDCl}_3$ )  $\delta$  36.6, 56.4, 57.6, 103.6, 114.8, 116.2, 120.8, 125.8, 125.9, 128.3, 128.5, 131.5, 137.6, 139.6, 140.4, 142.8, 149.8, 151.9, 161.9; MS  $m/z$  (%) 295 (97)  $[M]^+$ , 294 (89), 280 (100); HRMS (FAB)  $m/z$  calcd for  $\text{C}_{18}\text{H}_{17}\text{NO}_3$  (M) $^+$  295.1209, found 295.1200.

**1-(2-Hydroxy-3,4-dimethoxybenzyl)isoquinoline (3e').** Colorless oil;  $^1\text{H}$  NMR (200 MHz,  $\text{CDCl}_3$ )  $\delta$  3.77 (s, 3H), 3.89 (s, 3H), 4.55 (s, 2H), 6.36 (d, 1H,  $J = 8.5$  Hz), 6.94 (d, 1H,  $J = 8.5$  Hz), 7.55 (d, 1H,  $J = 6.0$  Hz), 7.62–7.73 (m, 2H), 7.81 (d, 1H, 7.9 Hz), 8.33–8.41 (m, 2H);  $^{13}\text{C}$  NMR (50 MHz,  $\text{CDCl}_3$ )  $\delta$  35.6, 55.9, 60.8, 103.3, 109.9, 118.9, 120.4, 124.2, 125.6, 126.9, 127.6, 127.9, 130.7, 131.1, 137.1, 139.4, 150.3, 160.9; MS  $m/z$

(%) 295 (22)  $[M]^+$ , 293 (27), 280 (100); HRMS (FAB)  $m/z$  calcd for  $\text{C}_{18}\text{H}_{17}\text{NO}_3$  (M) $^+$  295.1209, found 295.1222.

**1-(2-Hydroxy-3,4,5-trimethoxybenzyl)isoquinoline (3f).** Colorless oil;  $^1\text{H}$  NMR (200 MHz,  $\text{CDCl}_3$ )  $\delta$  3.76 (s, 3H), 3.82 (s, 3H), 3.94 (s, 3H), 4.53 (s, 2H), 6.58 (s, 1H), 7.56 (d, 1H,  $J = 6$  Hz), 7.64–7.85 (m, 3H), 8.36–8.43 (m, 2H);  $^{13}\text{C}$  NMR (50 MHz,  $\text{CDCl}_3$ )  $\delta$  31.6, 55.8, 60.4, 122.5, 123.6, 127.2, 128.1, 128.5, 128.8, 129.1, 129.3, 132.5, 136.3, 136.4, 146.5, 152.9; MS  $m/z$  (%) 325 (100)  $[M]^+$ , 168 (72), 167 (79); HRMS (FAB)  $m/z$  calcd for  $\text{C}_{19}\text{H}_{19}\text{NO}_4$  (M) $^+$  325.1314, found 325.1325.

**Sensitization and Quenching Experiments.** Solutions were prepared as described in the general procedure for irradiations and the concentration of quencher or sensitizer was adjusted as stated in the text. Photolyzates were analyzed by chromatography, as described above.

**Acknowledgment.** The authors acknowledge financial support from Spain's DGES (Project PB97-1077) and DGI (Project BQU2001-1890).

**Supporting Information Available:** Experimental details for the synthetic work and characterization data for all compounds. This material is available free of charge via the Internet at <http://pubs.acs.org>.

JO034074F